

Altermagnetic Anomalous Hall Effect Emerging from Electronic Correlations

Toshihiro Sato,^{1,2} Sonia Haddad,^{3,1,4} Ion Cosma Fulga,^{1,2} Fakhre F. Assaad,^{5,2} and Jeroen van den Brink^{1,2}

¹*Institute for Theoretical Solid State Physics, IFW Dresden, 01069 Dresden, Germany*

²*Würzburg-Dresden Cluster of Excellence ct.qmat, Germany*

³*Laboratoire de Physique de la Matière Condensée, Faculté des Sciences de Tunis, Université Tunis El Manar, Campus Universitaire 1060 Tunis, Tunisia*

⁴*Max-Planck-Institut für Physik komplexer Systeme, 01187 Dresden, Germany*

⁵*Institut für Theoretische Physik und Astrophysik, Universität Würzburg, 97074 Würzburg, Germany*

(Dated: September 5, 2024)

While altermagnetic materials are characterized by a vanishing net magnetic moment, their symmetry in principle allows for the existence of an anomalous Hall effect. Here, we introduce a model with altermagnetism in which the emergence of an anomalous Hall effect is driven by interactions. This model is grounded in a modified Kane-Mele framework with antiferromagnetic spin-spin correlations. Quantum Monte Carlo simulations show that the system undergoes a finite temperature phase transition governed by a primary antiferromagnetic order parameter accompanied by a secondary one of Haldane type. The emergence of both orders turns the metallic state of the system, away from half-filling, to an altermagnet with a finite anomalous Hall conductivity. A mean field ansatz corroborates these results, which pave the way into the study of correlation induced altermagnets with finite Berry curvature.

Introduction — Ferromagnetic conductors are generally endowed with an observable anomalous Hall effect (AHE), where an electric current perpendicular to the magnetization gives rise to a transversal Hall potential [1]. Here, the magnetization of the ferromagnet takes over the role of an external magnetic field that is the root cause of the standard Hall response in time-reversal invariant (i.e. nonmagnetic) conductors. On this basis one might expect that in a fully compensated antiferromagnet the lack of a net magnetization forces the AHE response to vanish. Interestingly, a symmetry analysis shows that this is not necessarily the case — only time-reversal symmetry breaking by itself is a sufficient condition to allow for an AHE, also in the absence of a net ferromagnetic moment. However, the combination of time-reversal *and* translation symmetry, which characterizes most antiferromagnetic materials, implies a vanishing AHE. Altermagnets comprise the class of compensated collinear antiferromagnets without this combined symmetry [2–8] and a large set of altermagnetic materials have been identified by first principles electronic structure calculations [9, 10]. They are characterized by a fully compensated magnetic order and therefore a zero net magnetic moment, but their symmetry properties reveal that this type of compensated magnetic order may induce an AHE [2, 11–15].

In spite of the clear ground-state symmetry considerations, so far no interacting models have been proposed in which an altermagnetic AHE emerges. The latter requires a time-reversal invariant Hamiltonian in which time-reversal symmetry (TRS) is spontaneously broken with zero total moment and still finite anomalous Hall conductivity. Here we show that precisely such an altermagnetic order emerges in a modified Kane-Mele model with broken inversion symmetry and antiferromagnetic

spin-spin interactions. Quantum Monte Carlo calculations reveal that, at finite temperature, the primary antiferromagnetic (AFM) order parameter gives rise to a secondary altermagnetic one, inducing a finite AHE. The occurrence of these two order parameters is in full agreement with the recently developed Landau theory of altermagnetism [16]. The smoking gun of this emergent altermagnetic phase is a spin-split electronic band structure with an anomalous Hall conductivity that can be tuned by doping.

Interacting altermagnetic Kane-Mele model — We start with a modified Kane-Mele (KM) model on a honeycomb lattice with a unit cell containing two sites denoted by A and B. In contrast to the canonical KM model, the sign of the complex phase of the hopping integrals between next nearest neighboring (NNN) sites is opposite on the two sublattices, as in Ref. [17]. The corresponding Hamiltonian is

$$\hat{H}_0 = -t \sum_{\langle i,j \rangle, s} \hat{c}_{i,s}^\dagger \hat{c}_{j,s} - \lambda \sum_{\langle\langle i,j \rangle\rangle, s} e^{is\Phi_{i,j}} \hat{c}_{i,s}^\dagger \hat{c}_{j,s} - \mu \sum_{i,s} \hat{n}_{i,s}, \quad (1)$$

where $\hat{c}_{i,s}$ is the annihilation operator of an electron of spin s on a honeycomb lattice site, $\hat{n}_{i,s} \equiv \hat{c}_{i,s}^\dagger \hat{c}_{i,s}$, and μ is the chemical potential. t and λ are the hopping integrals between the nearest neighboring (NN) and NNN sites, respectively. $\Phi_{i,j} = \pm\pi/2$ is the complex phase gained by an electron during a NNN hopping process according to the pattern shown in Fig. 1 (a). Effectively the λ term introduces a pseudoscalar potential that offsets the Dirac cones for the two spin components, thus generating anisotropic spin-split electronic bands [see Fig. 1 (b)]. For any finite value of λ , the SU(2) total spin symmetry is reduced to a U(1) one, and the inversion symmetry is broken, while TRS remains unbroken. Note that

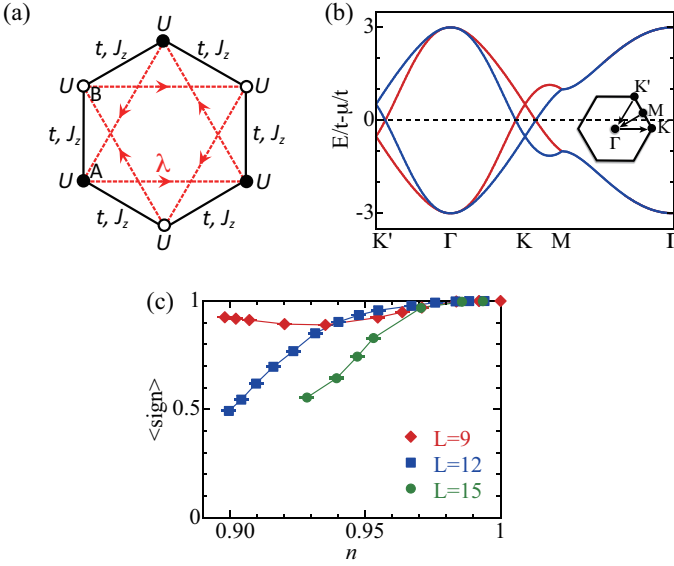


FIG. 1. (a) The model of fermions on the honeycomb lattice with hopping (t , λ) and interaction (J_z , U) terms in Eq. (2). (b) Noninteracting band structure at $\lambda = 0.1$ for the half-filled case. The red (blue) line corresponds to the spin-up (spin-down) component. Inset: the first Brillouin zone is depicted and the black lines indicate the scans considered here. (c) Quantum Monte Carlo average sign, $\langle \text{sign} \rangle$, as a function of L for various electron densities n at temperature $T = 1/20$.

the canonical KM model maintains both time-reversal and inversion symmetries, resulting in degenerate spin states without spin splitting. For an altermagnetic state to emerge, spin-spin interactions must maintain zero net magnetization while they spontaneously break TRS. Accordingly we consider an AFM interaction term, ensuring that each spin on one sublattice is coupled exclusively to spins on the opposing sublattice. The total Hamiltonian, taking into account an appropriate interaction that realizes the aforementioned physical characteristics, reads

$$\hat{H} = \hat{H}_0 - \frac{J_z}{2} \sum_{\langle i,j \rangle} (\hat{S}_i^z - \hat{S}_j^z)^2, \quad (2)$$

where $\hat{S}_i^z = \frac{1}{2} \sum_{\sigma\sigma'} \hat{c}_{i\sigma}^\dagger \sigma^z \hat{c}_{i\sigma'}$ is the fermion spin operator and σ corresponds to the vector of Pauli spin-1/2 matrices. We consider $J_z > 0$ such that the $\hat{S}_i^z \hat{S}_j^z$ term harbors the potential for the development of long-range AFM order in the spin- z direction. In addition an effective on-site Hubbard repulsion term $U \sum_i \hat{n}_{i\uparrow} \hat{n}_{i\downarrow}$ with $U = \frac{3J_z}{4}$ is generated, which preempts any local pairing instability.

Symmetry analysis — To establish that the effective Landau theory of our model is of altermagnetic nature [18], we consider the continuum limit where the low energy effective Hamiltonian is

$$H_0^{\text{eff}} = \sum_k \Psi_k^\dagger (k_x \tau^x \mu^z - k_y \tau^y) \Psi_k + \lambda \sum_k \Psi_k^\dagger \mu^z \sigma^z \Psi_k.$$

Here $\Psi_k^\dagger = \Psi_{k,\tau,\mu,\sigma}^\dagger$ and τ, μ, σ account for the sublattice, valley and spin indices, respectively, on which the Pauli matrices $\tau^\alpha, \mu^\alpha, \sigma^\alpha$ act. The first term corresponds to the Dirac Hamiltonian of graphene with unit Fermi velocity and the second term to the NNN hopping of the lattice model. Importantly, we note that this term differs from the quantum spin Hall mass, which takes the form $\sum_k \Psi_k^\dagger \mu^z \tau^z \sigma^z \Psi_k$ [19]. It does not open a gap in the spectrum, but shifts the valleys in energy by $\lambda \mu^z \sigma^z$, as is seen in Fig. 1(b). The Hamiltonian is invariant under global $U(1)$ spin rotations around the z axis, while discrete symmetries include time reversal: $T^{-1} \alpha \Psi_k^\dagger T = \bar{\alpha} \Psi_{-k}^\dagger \mu^x i \sigma^y$, where $\bar{\alpha}$ denotes the complex conjugation of the α . Importantly, the λ term breaks inversion symmetry: $I^{-1} \alpha \Psi_k^\dagger I = \alpha \Psi_{-k}^\dagger \tau^x \mu^x$. The interaction term generates

$$H_I = -J_z \int d^2 \mathbf{x} \left(\Psi^\dagger(\mathbf{x}) \sigma^z \tau^z \Psi(\mathbf{x}) \right)^2, \quad (3)$$

which does not lower the symmetry of the model, and clearly promotes antiferromagnetism. To proceed, we now consider a symmetry broken antiferromagnetic state in the spin- z direction described by the collinear Néel order parameter

$$N_{\parallel}(\mathbf{x}) = \left\langle \Psi^\dagger(\mathbf{x}) \sigma^z \tau^z \Psi(\mathbf{x}) \right\rangle. \quad (4)$$

This order parameter solely breaks TRS such that a Ginzburg-Landau theory accounting for this state can include even powers of $N(\mathbf{x})$. However, terms of the form $N(\mathbf{x})M(\mathbf{x})$ are also allowed in the Ginzburg-Landau functional provided that $M(\mathbf{x})$ is odd under time reversal and that $N(\mathbf{x})M(\mathbf{x})$ shares the same symmetries as the Hamiltonian. This requirement is fulfilled by the Haldane mass [20]

$$M_H(\mathbf{x}) = \left\langle \Psi^\dagger(\mathbf{x}) \tau^z \mu^z \Psi(\mathbf{x}) \right\rangle \quad (5)$$

which indeed is odd under time reversal and generates the AHE. Since at $\lambda \neq 0$ the Hamiltonian does not enjoy inversion symmetry, $N_{\parallel}(\mathbf{x})M_H(\mathbf{x})$ is allowed in the Ginzburg-Landau theory. As a consequence, as soon as $N_{\parallel}(\mathbf{x})$ acquires a nontrivial expectation value, the Haldane mass is generated as a secondary order parameter [18]. We note that at half-band filling, characterized by the particle-hole symmetry $P^{-1} \alpha \Psi_k^\dagger P = \bar{\alpha} \Psi_k^\dagger \tau^z \sigma^x$, the linear coupling between the two order parameters is forbidden since N_{\parallel} is even and M_H is odd under this symmetry. It is worth stressing that in the case of an in-plane magnetic ordering, the Ginzburg-Landau formulation will be rephrased in terms of a two-component primary order parameter $\mathbf{N}_{\perp}(\mathbf{x}) = \left\langle \Psi^\dagger(\mathbf{x}) \tau^z (\sigma^x, \sigma^y) \Psi(\mathbf{x}) \right\rangle$, which breaks $U(1)$ spin symmetry as well as TRS. As a consequence, it cannot be linearly coupled to the scalar secondary order parameter $M_H(\mathbf{x})$, forbidding by symmetry the emergence of $M_H(\mathbf{x})$ and the subsequent altermagnetic properties.

On the lattice, it is clear that the model harbors magnetism beyond simple AFM order as the collinear AFM ordered spin state on the two sublattices cannot be connected by a translation or inversion symmetry combined with time reversal, due to the specific phase patterns in the NNN hopping Hamiltonian, as is expected for an altermagnet [5]. Indeed, we will show that this results in a finite total Berry curvature away from half-filling, in sync with the finite Haldane mass in the continuum description.

Quantum Monte Carlo results — The Hamiltonian (2) was simulated using the ALF (Algorithms for Lattice Fermions) implementation [21, 22] of the grand-canonical, finite-temperature, auxiliary-field quantum Monte Carlo method [23–25]. In fact the interaction part of Eq. (2) in terms of perfect squares can be implemented in the ALF implementation. Results were obtained on lattices with $L \times L$ unit cells ($2L^2$ sites) and periodic boundary conditions. Henceforth, we use $t = 1$ as the energy unit, set $\lambda = 0.1$, $J_z = 2$ and set the Trotter imaginary time step to $\Delta\tau = 0.1$. The negative sign problem is absent at half-filling since in a Bogoliubov basis, $(\hat{\gamma}_{i,\uparrow}^\dagger, \hat{\gamma}_{i,\downarrow}^\dagger) = (\hat{c}_{i,\uparrow}^\dagger, (-1)^i \hat{c}_{i,\downarrow}^\dagger)$, and after decoupling the perfect square term with a Hubbard-Stratonovitch transformation, time-reversal and $U(1)$ charge symmetries are present for each field configuration [26]. Doping breaks this symmetry and the sign problem sets in. Nevertheless, for our specific implementation it turns out to be mild [see Fig. 1 (c)] such that *large* lattices and *low* temperatures can be reached. In particular, we are able to reveal an altermagnetic phase, as shown in Fig. 2. In fact, this was achieved by viewing the sign problem as an optimization problem over the space of possible path integral formulations.

To verify the above low-energy theory, we measure equal-time correlation functions

$$C^O(\mathbf{q}) \equiv \frac{1}{L^2} \sum_{\mathbf{r}, \mathbf{r}'} \langle \hat{O}_{\mathbf{r}}^O \hat{O}_{\mathbf{r}'}^O \rangle e^{i\mathbf{q} \cdot (\mathbf{r} - \mathbf{r}')} \quad (6)$$

of fermion spin $\hat{O}_{\mathbf{r}}^{S_z(S_{xy})} = \hat{S}_{\mathbf{r},A}^{z(xy)} - \hat{S}_{\mathbf{r},B}^{z(xy)}$ with $\hat{S}_{\mathbf{r}}^s = \frac{1}{2} \hat{c}_{\mathbf{r}}^\dagger \sigma^s \hat{c}_{\mathbf{r}}$, and the operator corresponding to the Haldane mass, $\hat{O}_{\mathbf{r}}^{\text{AH}} = \sum_{\langle\langle \delta, \delta' \rangle\rangle, \sigma} e^{i\Phi_{\mathbf{r}+\delta, \mathbf{r}+\delta'}} \hat{c}_{\mathbf{r}+\delta, \sigma}^\dagger \hat{c}_{\mathbf{r}+\delta', \sigma}$. Here, \mathbf{r} specifies a unit cell, or hexagon, and $\langle\langle \delta, \delta' \rangle\rangle$ runs over the NNN sites of this hexagon. After computing the correlation functions, we extracted the renormalization-group invariant correlation ratios [27, 28]

$$R^O = 1 - \frac{C^O(\mathbf{q}_0 + \delta\mathbf{q})}{C^O(\mathbf{q}_0)}. \quad (7)$$

Here \mathbf{q}_0 is the ordering wave vector and $\mathbf{q}_0 + \delta\mathbf{q}$ the longest wave-length fluctuation of the ordered state for a given lattice size. Long-range AFM and anomalous Hall (AH) orders here imply a divergence of the corresponding correlation functions $C^O(\mathbf{q}_0 = 0)$. Accordingly, $R^O \rightarrow 1$

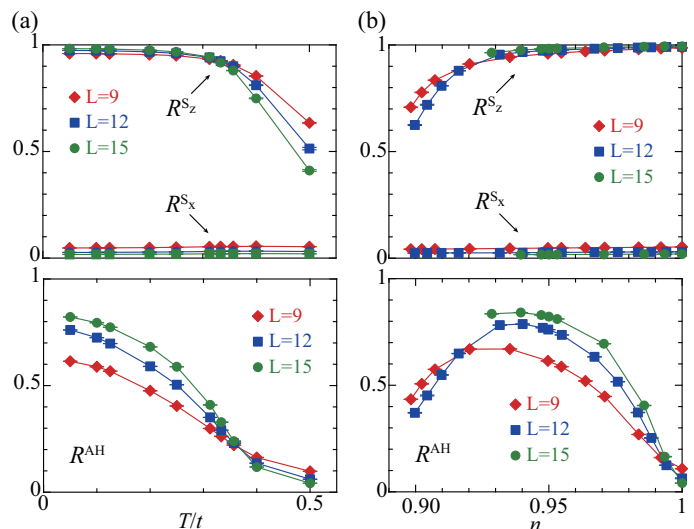


FIG. 2. (a) Temperature dependence of correlation ratios for z -AFM and x -AFM orders (top panel) and AH order (bottom panel) at electron density $n = 0.95$. Here, L is the system size, $\lambda = 0.1$ and $J_z = 2$ in units of t . (b) Same as (a) for varying electron density n at temperature $T = 1/20$.

for $L \rightarrow \infty$ in the ordered phase, whereas $R^O \rightarrow 0$ in the disordered phase. At the critical point, R^O becomes scale-invariant for sufficiently large system size L , leading to a crossing of results for different L .

We find the altermagnetic phase in the range of parameters, specifically temperatures T and electron densities n , shown in Fig. 2. Figure 2 (a) shows the results as a function of T at $n = 0.95$. The onset of the AFM in spin- z (x) direction, termed z -AFM (x -AFM), is detected from the crossing of R^{S_z} (R^{S_x}), whereas the onset of the AH order can be detected from R^{AH} . As the temperature decreases, we observe the onset of the z -AFM order. We note that z -AFM only breaks time-reversal symmetry such that ordering at finite temperature is allowed. A key feature is that its appearance coincides with the onset of the AH order. Indeed, the data for R^{AH} are consistent with a finite-temperature phase transition to the z -AFM phase. Furthermore, within the range of parameters we investigated, we do not observe the emergence of the x -AFM order. Results as a function of n for $T = 1/20$ are presented in Fig. 2 (b). The consequence of the simultaneous emergence of both z -AFM and AH orders persists against changes in electron density away from half filling. At half-filling the z -AFM ordering persists while AH correlations are suppressed. This agrees with our finding of a vanishing linear coupling between the AH and z -AFM order in the Ginzburg-Landau functional when particle-hole symmetry is present. As n is further decreased, the correlation ratios do not provide clear evidence of both these orders, transitioning to the disordered phase.

We conclude this section by noting that we have checked that no ferromagnetic order emerges, such that

the state that we observe is a compensated collinear antiferromagnet.

AHE in mean field approximation — Within a mean field (MF) approximation the AHE that emerges in the interacting modified KM model can be accessed directly. Using the spin-dependent sublattice basis $(\psi_{A\uparrow}, \psi_{B\uparrow}, \psi_{A\downarrow}, \psi_{B\downarrow})$, the corresponding Hamiltonian, given by Eq. (2), reduces to

$$H^{\text{MF}}(\mathbf{k}) = (\epsilon - \mu)\sigma^0\tau^0 + a_{\mathbf{k}}\tau^0\sigma^z + \mathbf{h}(\mathbf{k}) \cdot \boldsymbol{\tau}, \quad (8)$$

where $h(\mathbf{k}) = (b_{\mathbf{k}}\sigma^0, c_{\mathbf{k}}\sigma^0, h_z)$, $h_z = -\Delta M_z^{\text{AFM}}\sigma^z$, $\Delta = \frac{3}{2}J_z + \frac{3}{4}|J_z|$, μ is the chemical potential, $\epsilon = \frac{3}{8}|J_z|(n-1)$, $n = n_a = n_b$ is the electron density on site A or B, with $n_l = \langle \hat{n}_{l\uparrow} \rangle + \langle \hat{n}_{l\downarrow} \rangle$, $l = a, b$ being the sublattice index. The antiferromagnetic M_z^{AFM} order parameter along the z direction is expressed in terms of the on-site magnetization as $M_z^{\text{AFM}} = \frac{1}{2}(m_z^a - m_z^b)$, where $m_z^l = \frac{1}{2}(\langle \hat{n}_{l\uparrow} \rangle - \langle \hat{n}_{l\downarrow} \rangle)$. The hopping terms $a_{\mathbf{k}}$, $b_{\mathbf{k}}$ and $c_{\mathbf{k}}$ are given by $a_{\mathbf{k}} = -2\lambda \sum_{i=1}^3 \sin(\mathbf{k} \cdot \mathbf{a}_i)$, $b_{\mathbf{k}} = -t \sum_{i=1}^3 \cos(\mathbf{k} \cdot \boldsymbol{\delta}_i)$, $c_{\mathbf{k}} = -t \sum_{i=1}^3 \sin(\mathbf{k} \cdot \boldsymbol{\delta}_i)$. $\boldsymbol{\delta}_i$ and \mathbf{a}_i are, respectively, the vectors connecting NN and NNN sites; $\mathbf{a}_1 = \sqrt{3}a(-\frac{1}{2}, \frac{\sqrt{3}}{2})$, $\mathbf{a}_2 = \sqrt{3}a(-\frac{1}{2}, -\frac{\sqrt{3}}{2})$, $\mathbf{a}_3 = \sqrt{3}a(1, 0)$, $\boldsymbol{\delta}_1 = a(\frac{\sqrt{3}}{2}, \frac{1}{2})$, $\boldsymbol{\delta}_2 = a(-\frac{\sqrt{3}}{2}, \frac{1}{2})$, $\boldsymbol{\delta}_3 = a(0, -1)$, where a is the distance between NN sites. τ^0 (σ^0) is the 2×2 identity matrix in the sublattice (spin) space.

The spectrum of the mean field Hamiltonian (8) is given by

$$E_{\nu,\sigma}^{\text{MF}}(\mathbf{k}) = \epsilon - \mu + a_{\mathbf{k}}\sigma + \nu\sqrt{b_{\mathbf{k}}^2 + c_{\mathbf{k}}^2 + (\Delta M_z^{\text{AFM}})^2},$$

where $\nu = \pm$ ($\sigma = \pm$) is the band (spin) index. The spin-dependent mass term h_z in Eq. (8) breaks TRS and a nonvanishing Berry curvature (BC) is expected away from half-filling. For a given spin projection σ , the BC of a band ν can be expressed as [29, 30]

$$\Omega_z^\nu(\sigma, \mathbf{k}) = -\frac{\nu}{2|\mathbf{h}(\mathbf{k})|^3} \mathbf{h}(\mathbf{k}) \cdot [\partial_{k_x} \mathbf{h}(\mathbf{k}) \times \partial_{k_y} \mathbf{h}(\mathbf{k})]$$

and the AH conductivity [7] is given by the integral

$$\sigma_{\text{Hall}} = -\frac{e^2}{\hbar} \frac{1}{(2\pi)^2} \sum_{\sigma,\nu} \int_{BZ} d\mathbf{k} \Omega_z^\nu(\sigma, \mathbf{k}) f_\nu(\mathbf{k}, \mu),$$

where $h(\mathbf{k}) = (b_{\mathbf{k}}, c_{\mathbf{k}}, -\Delta M_z^{\text{AFM}}\sigma)$ and $f_\nu(\mathbf{k}, \mu)$ is the Fermi-Dirac distribution function [31].

σ_{Hall} can be computed using the values of the chemical potential and the AFM magnetization M_z^{AFM} extracted from the mean field calculations. The results are depicted in Fig. 3 showing σ_{Hall} as function of the electronic density n .

The occurrence of a nonvanishing AH conductivity can be understood from the spin-valley dependence of the BC and the offset of the Dirac points induced by the modified KM term $a_{\mathbf{k}}\sigma^z\tau^0$ of Eq. (8), which shifts oppositely the spin-split bands. To gain further insight into these features, let us focus on the states $\mathbf{k} = \mu_z \mathbf{K} + \mathbf{q}$, ($\mathbf{q} \ll |\mathbf{K}|$)

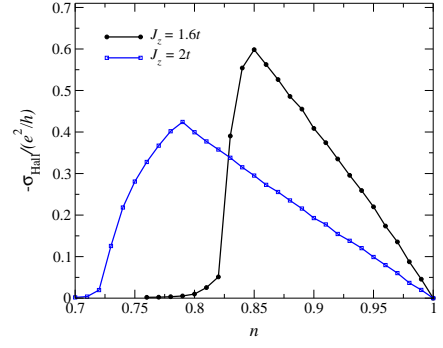


FIG. 3. Anomalous Hall conductivity σ_{Hall} in units of e^2/h as a function of the electron density n for $J_z = 1.6t$ and $J_z = 2t$ using the mean field parameters for n and M_z^{AFM} .

in the vicinity of the Dirac points $\mu_z \mathbf{K}$, where $\mu_z = \pm$ is the valley index. These states contribute strongly to the BC, which reduces, around $\mu_z \mathbf{K}$, to

$$\Omega_z^\nu(\sigma, \mu_z, \mathbf{q}) = \text{sgn} \frac{(\hbar v_F)^2 \Delta M_z^{\text{AFM}}}{2 [(\hbar v_F \mathbf{q})^2 + (\Delta M_z^{\text{AFM}})^2]^{3/2}}, \quad (9)$$

where $\text{sgn} = -\nu\mu_z\sigma$ is the sign of the BC and $\hbar v_F = \frac{3}{2}at$. Given the spin-dependent offset of the Dirac points, a spin-split subband $E_{\nu,\sigma}^{\text{MF}}(\mathbf{k})$ [$E_{\nu,-\sigma}^{\text{MF}}(\mathbf{k})$] of an occupied band ν , contributes to the BC by the states around the valley μ^z ($-\mu^z$). Thus, the two contributing spin-dependent BCs have the same sign, resulting in a nonvanishing total BC away from half-filling. Data are shown in the Supplemental Material [32]. We note that in the continuum limit, our modified KM term, $a_{\mathbf{k}}\tau^0\sigma^z$, indeed corresponds to a valley-Zeeman spin-orbit coupling, akin to that considered in transition metal dichalcogenides [33, 34]. Both systems exhibit effects that induce spin-split band structures and enable spin-valley locking, but their underlying origins differ, as detailed in the Supplemental Material [32].

The doping dependence of the AH conductivity (see Fig. 3) reflects the behavior of the secondary order parameter of Haldane type M_H . At half-filling ($n = 1$), σ_{Hall} vanishes as the bands below the Fermi level are fully occupied, resulting in zero total BC. Decreasing n from half-filling, $|\sigma_{\text{Hall}}|$ increases up to a maximum value, at a doping n_c , where it drops and vanishes below a critical doping value n_{c0} . Larger coupling constants J_z give smaller n_{c0} . For a fixed J_z , the increase of $|\sigma_{\text{Hall}}|$ can be understood from the BC contribution which is enhanced as the area of the spin-polarized Fermi surface increases (see the Supplemental Material [32]). The drop of $|\sigma_{\text{Hall}}|$ is a consequence of the sharp decrease of M_z^{AFM} below n_c , inducing a decrease of the BC. The doping regime with a nonzero AH conductivity gets wider as J_z increases, which results from the enhancement of the mass term M_z^{AFM} .

Conclusions and outlook — We have shown how elec-

tronic interactions induce altermagnetism in a noncentrosymmetric system by stabilizing a primary AFM ordering that hosts a secondary one that directly induces the altermagnetic anomalous Hall effect. Specifically, our quantum Monte Carlo calculations on the interacting modified Kane-Mele lattice model reveal a finite temperature phase transition into an altermagnetically ordered state, whose physical features are captured by its effective continuum theory. The interacting model may in principle be implemented in cold atoms in optical lattices that have been proposed to realize altermagnetism [35]. Time-modulated optical lattices of ultracold atoms allow for complex NNN tunneling, as demonstrated for the Haldane model [36], while Hubbard models with AFM order have been realized in ultracold fermions [37, 38]. This suggests potential for combining these techniques, incorporating both complex NNN tunneling and Hubbard-type models with AFM order. Interestingly, recently an experimental realization of a non-centrosymmetric 3D altermagnet has been reported in GdAlSi, a collinear antiferromagnetic Weyl semimetal [39]. This suggests generalization of the lattice model to higher dimensions to determine how electronic correlations generate Berry curvature in altermagnetic semimetals that may as well harbor 3D electronic topology.

Acknowledgments — We acknowledge fruitful discussions with Paul McClarty, Olena Gomonay, Libor Šmejkal, and Tomáš Jungwirth. We gratefully acknowledge the Gauss Centre for Supercomputing e.V. for funding this project by providing computing time on the GCS Supercomputer SUPERMUC-NG at Leibniz Supercomputing Centre, (project No. pn73xu) as well as the scientific support and HPC resources provided by the Erlangen National High Performance Computing Center (NHR@FAU) of the Friedrich-Alexander-Universität Erlangen-Nürnberg (FAU) under the NHR project b133ae. NHR funding is provided by federal and Bavarian state authorities. NHR@FAU hardware is partially funded by the German Research Foundation (DFG) — 440719683. FA, TS, JvdB and ICF thank the Würzburg-Dresden Cluster of Excellence on Complexity and Topology in Quantum Matter ct.qmat (EXC 2147, project-id 390858490). S. H. acknowledges the Institute for Theoretical Solid State Physics at IFW (Dresden) and the Max Planck Institute for the Physics of Complex Systems (Dresden) for kind hospitality and financial support.

[1] N. Nagaosa, J. Sinova, S. Onoda, A. H. MacDonald, and N. P. Ong, *Rev. Mod. Phys.* **82**, 1539 (2022).
 [2] L. Šmejkal, R. González-Hernández, T. Jungwirth, and J. Sinova., *Sci. Adv.* **6**, eaaz8809 (2020).

[3] S. Hayami, Y. Yanagi, and H. Kusunose, *J. Phys. Soc. Jpn.* **88**, 123702 (2019).
 [4] L.-D. Yuan, Z. Wang, J.-W. Luo, E. I. Rashba, and A. Zunger, *Phys. Rev. B* **102**, 014422 (2020).
 [5] L. Šmejkal, J. Sinova, and T. Jungwirth, *Phys. Rev. X* **12**, 031042 (2022).
 [6] I. I. Mazin, K. Koepernik, M. D. Johannes, R. González-Hernández, and L. Šmejkal, *PNAS* **118**, e2108924118 (2021).
 [7] L. Šmejkal, A. H. MacDonald, J. Sinova, S. Nakatsuji, and T. Jungwirth, *Nat. Rev. Mater.* **7**, 482 (2022), [arXiv:2107.03321](https://arxiv.org/abs/2107.03321).
 [8] L. Šmejkal, J. Sinova, and T. Jungwirth, *Phys. Rev. X* **12**, 040501 (2022).
 [9] Y. Guo, H. Liu, O. Janson, I. C. Fulga, J. van den Brink, and J. I. Facio, *Mater. Today Phys.* **32**, 100991 (2023).
 [10] I. Mazin, R. González-Hernández, and L. Šmejkal, [arXiv:2309.02355](https://arxiv.org/abs/2309.02355) (2023), [10.48550/arXiv.2309.02355](https://arxiv.org/abs/2309.02355).
 [11] R. González-Hernández, L. Šmejkal, K. Výborný, Y. Yahagi, J. Sinova, T. Jungwirth, and J. Železný, *Phys. Rev. Lett.* **126**, 127701 (2021).
 [12] Z. Feng, X. Zhou, L. Šmejkal, L. Wu, Z. Zhu, H. Guo, R. González-Hernández, X. Wang, H. Yan, P. Qin, X. Zhang, H. Wu, H. Chen, Z. Meng, L. Liu, Z. Xia, J. Sinova, T. Jungwirth, and Z. Liu, *Nat. Electron* **5**, 735 (2022).
 [13] R. D. G. Betancourt, J. Zubáč, R. González-Hernández, K. Geishendorf, Z. Šobán, G. Springholz, K. Olejník, L. Šmejkal, J. Sinova, T. Jungwirth, S. T. B. Goennenwein, A. Thomas, H. Reichlová, J. Železný, and D. Krieger, *Phys. Rev. Lett.* **130**, 036702 (2023).
 [14] H. Bai, L. Han, X. Y. Feng, Y. J. Zhou, R. X. Su, Q. W. L. Y. Liao, W. X. Zhu, X. Z. Chen, F. Pan, X. L. Fan, and C. Song, *Phys. Rev. Lett.* **128**, 197202 (2022).
 [15] S. Reimers, L. Odenbreit, L. Šmejkal, V. N. Strocov, P. Constantinou, A. B. Hellenes, R. J. Ubierno, W. H. Campos, V. K. Bharadwaj, A. Chakraborty, T. Denneulin, W. Shi, R. E. Dunin-Borkowski, S. Das, M. Kläui, J. Sinova, and M. Jourdan, [arXiv:2310.17280](https://arxiv.org/abs/2310.17280) (2023), [10.48550/arXiv.2310.17280](https://arxiv.org/abs/2310.17280).
 [16] P. A. McClarty and J. G. Rau, *Phys. Rev. Lett.* **132**, 176702 (2024).
 [17] E. Colomé and M. Franz, *Phys. Rev. Lett.* **120**, 086603 (2018).
 [18] P. A. McClarty and J. G. Rau, [arXiv:2308.04484](https://arxiv.org/abs/2308.04484) (2023), [10.48550/arXiv.2308.04484](https://arxiv.org/abs/2308.04484).
 [19] C. L. Kane and E. J. Mele, *Phys. Rev. Lett.* **95**, 226801 (2005).
 [20] F. D. M. Haldane, *Phys. Rev. Lett.* **61**, 2015 (1988).
 [21] M. Bercx, F. Goth, J. S. Hofmann, and F. F. Assaad, *SciPost Phys.* **3**, 013 (2017).
 [22] F. F. Assaad, M. Bercx, F. Goth, A. Götz, J. S. Hofmann, E. Huffman, Z. Liu, F. P. Toldin, J. S. E. Portela, and J. Schwab, *SciPost Phys. Codebases*, **1** (2022).
 [23] R. Blankenbecler, D. J. Scalapino, and R. L. Sugar, *Phys. Rev. D* **24**, 2278 (1981).
 [24] S. White, D. Scalapino, R. Sugar, E. Loh, J. Gubernatis, and R. Scalettar, *Phys. Rev. B* **40**, 506 (1989).
 [25] F. Assaad and H. Evertz, in *Computational Many-Particle Physics*, Lecture Notes in Physics, Vol. 739, edited by H. Fehske, R. Schneider, and A. Weiße (Springer, Berlin Heidelberg, 2008) pp. 277–356.
 [26] C. Wu and S.-C. Zhang,

- Phys. Rev. B **71**, 155115 (2005).
- [27] K. Binder, *Z. Phys. B Con. Mat.* **43**, 119 (1981).
- [28] S. Pujari, T. C. Lang, G. Murthy, and R. K. Kaul, *Phys. Rev. Lett.* **117**, 086404 (2016).
- [29] X.-L. Qi, T. L. Hughes, and S.-C. Zhang, *Phys. Rev. B* **78**, 195424 (2008).
- [30] A. Graf and F. Piéchon, *Phys. Rev. B* **104**, 085114 (2021).
- [31] To carry out the integration over the Brillouin zone, it is easier to use the mapping to a square Brillouin zone and write the Hamiltonian in terms of the variables $q_x = \mathbf{k} \cdot \mathbf{a}_3$ $q_y = \mathbf{k} \cdot \mathbf{a}_1$. The Dirac points are at $\mathbf{q}_D = \pm(2\pi/3, 2\pi/3)$. The δ_i vectors can be expressed as $\delta_i = \frac{1}{3}\epsilon_{ijk}(\mathbf{a}_k - \mathbf{a}_j)$ [40].
- [32] See Supplemental Material, which includes Refs. [17, 33, 34, 41, 42], for additional details on our mean field calculations and Berry curvatures, as well as a discussion of the relation between our model and valley-Zeeman spin-orbit coupling.
- [33] D. Xiao, G.-B. Liu, W. Feng, X. Xu, and W. Yao, *Phys. Rev. Lett.* **108**, 196802 (2012).
- [34] X. Wang, W. Yang, W. Yang, Y. Cao, X. Lin, G. Wei, H. Lu, P. Tang, and W. Zhao, *Applied Physics Reviews* **9**, 031402 (2022).
- [35] P. Das, V. Leeb, J. Knolle, and M. Knap, [arXiv:2312.10151](https://arxiv.org/abs/2312.10151) (2023), [10.48550/arXiv.2312.10151](https://doi.org/10.48550/arXiv.2312.10151).
- [36] G. Jotzu, M. Messer, R. Desbuquois, M. Lebrat, T. Uehlinger, D. Greif, and T. Esslinger, *Nature* **515**, 237 (2014).
- [37] R. A. Hart, P. M. Duarte, T.-L. Yang, X. Liu, T. Paiva, E. Khatami, R. T. Scalettar, N. Trivedi, D. A. Huse, and R. G. Hulet, *Nature* **519**, 211 (2015).
- [38] A. Mazurenko, C. S. Chiu, G. Ji, M. F. Parsons, M. Kanász-Nagy, R. Schmidt, F. Grusdt, E. Demler, D. Greif, and M. Greiner, *Nature* **545**, 462 (2017).
- [39] J. Nag, B. Das, S. Bhowal, Y. Nishioka, B. Bandyopadhyay, S. Kumar, K. Kuroda, A. Kimura, K. G. Suresh, and A. Alam, [arXiv:2312.11980v2](https://arxiv.org/abs/2312.11980v2) (2023), [10.48550/arXiv.2312.11980](https://doi.org/10.48550/arXiv.2312.11980).
- [40] D. Sticlet, F. Piéchon, J.-N. Fuchs, P. Kalugin, and P. Simon, *Phys. Rev. B* **85**, 165456 (2012).
- [41] J. Cayssol and J. N. Fuchs, *Journal of Physics: Materials* **4**, 034007 (2021).
- [42] X. Chen, L. Zhong, X. Li, and J. Qi, *Nanoscale* **9**, 2188 (2017).
- [43] Z. Y. Zhu, Y. C. Cheng, and U. Schwingenschlögl, *Phys. Rev. B* **84**, 153402 (2011).

$$\Omega_z^\alpha(\sigma, \mathbf{k}) = -\alpha\sigma \frac{\Delta M_z^{\text{AFM}}}{|\mathbf{h}(\mathbf{k})|^3} \sqrt{3}(at)^2 \sin\left(\mathbf{k} \cdot \frac{(\delta_2 - \delta_3)}{2}\right) \sin\left(\mathbf{k} \cdot \frac{(\delta_3 - \delta_1)}{2}\right) \sin\left(\mathbf{k} \cdot \frac{(\delta_1 - \delta_2)}{2}\right), \quad (15)$$

where $\alpha = \pm$ and $\sigma = \pm$ are, respectively, the band and the spin indices.

In Fig. 6 we plot the BC of the occupied spin sub-bands for a coupling constant $J_z = 2t$ and a doping $n = 0.79$, at which the anomalous Hall conductivity reaches its maximum. Figure 6 shows that, at the opposite valleys, the contributing bands with opposite spin projections have the same sign of the BC, which gives rise to a finite total Berry curvature of the occupied bands.

The doping dependence of the corresponding anomalous Hall conductivity is depicted in Fig. 3 in the main text. This behavior is reminiscent of that of the secondary order parameter denoted M_H ($= O_{\text{AH}}$ given in the main text) in Fig. 4. As shown in Fig. 3 of the main text, by decreasing n from half-filling, $|\sigma_{\text{Hall}}|$ increases up to a maximum value corresponding at a doping amplitude n_c below which it drops and vanishes at a critical doping value n_{c0} . The increase of $|\sigma_{\text{Hall}}|$ can be understood from the BC contribution which is enhanced as the area of the spin-polarized Fermi surface increases [see Fig. 4 for $0.79 < n < 1$]. The drop of $|\sigma_{\text{Hall}}|$ below n_c is due to two effects: (i) the sharp decrease of M_z^{AFM} [see Table I] and (ii) the contribution to the BC of two bands with opposite spin projections at a given valley [see Fig. 4 for $n < 0.79$]. In the case of Fig. 4, the larger the Fermi surface of the conduction band of spin $\sigma = -$ at the valley K , the smaller the BC.

Figure 7 shows the coupling and the doping ranges where emerge the order parameters in a non-vanishing anomalous Hall conductivity.

Valley-Zeeman spin-orbit coupling

In the continuum limit, our modified Kane-Mele term for the Hamiltonian of Eq. (1) in the main text,

$a_{\mathbf{k}}\tau^0\sigma^z$, reduces around a Dirac point, $\mathbf{k} = \mu_z\mathbf{K}$, to $-3\sqrt{3}\lambda\mu_z\sigma^z\tau^0$, where $\mu_z = \pm$ indicates the valley index. It is interesting to note that the resulting expression corresponds to a valley-Zeeman spin-orbit coupling (VZ-SOC), as observed in transition metal dichalcogenides (TMDs) [33, 34]. The VZ-SOC breaks inversion symmetry and induces, in monolayer TMD, a spin-split electronic band structure and a spin-valley locking effect, which gives rise to the valley anomalous Hall effect [33, 42]. While these phenomena are similar, their origins differ: in our case, the modified Kane-Mele term is characterized by a spin-dependent hopping process, while in TMD, it arises from the band structure formed by the coupling of transition metal d -orbitals and chalcogen p -orbitals [43], further influenced by atomic spin-orbit coupling that splits the bands.

Effect of Rashba spin-orbit coupling and repulsive Hubbard interaction

We present the mean-field results when an additional term is included in Eq.(2) of the main text. In Fig. 8(a) we show the results in the presence of a Rashba SOC which does not affect the altermagnetic properties of the system. Including the repulsive Hubbard U term demonstrates that the altermagnetism persists even when the coupling J_z is smaller than U and t , as shown in Fig. 8(b).

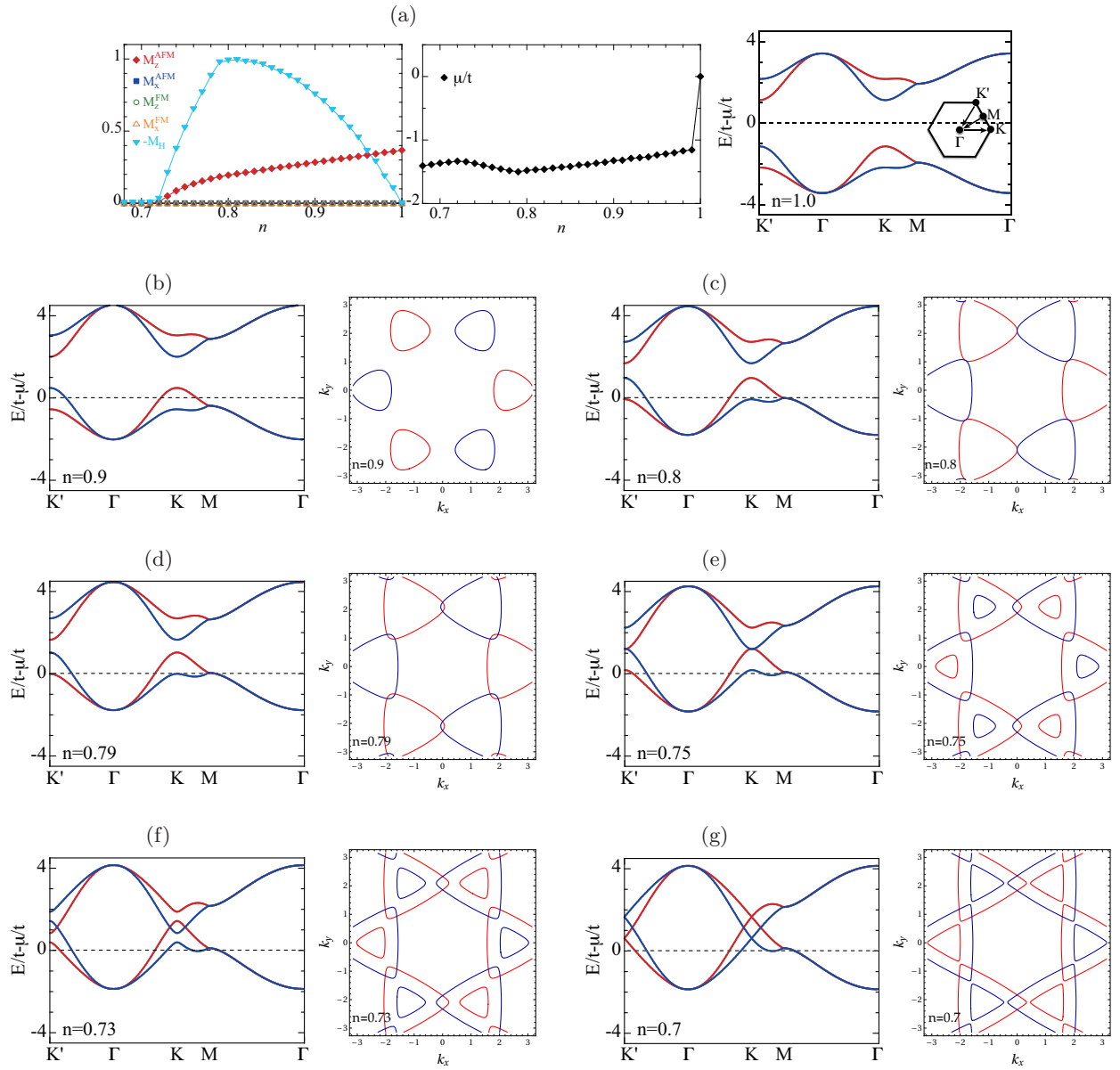


FIG. 4. Mean-field results for $\lambda = 0.1t$ and $J_z = 2t$. (a) Order parameters and chemical potential as a function of electron density n and band structures for $n = 1$. Inset: the first Brillouin zone is depicted and the black lines indicate the scans considered here. Band structures and corresponding Fermi surfaces for (b) $n = 0.9$, (c) $n = 0.8$, (d) $n = 0.79$, (e) $n = 0.75$, (f) $n = 0.73$, and (g) $n = 0.7$. The red (blue) line corresponds to the spin up (down) component.

n	1	0.9	0.8	0.79	0.75	0.73	0.7
M_z^{AFM}	0.3675933	0.2839518	0.1946018	0.1843236	0.1134823	0.0497554	0.0015749

TABLE I. Mean-field data of M_z^{AFM} at different doping levels n for $J_z = 2t$.

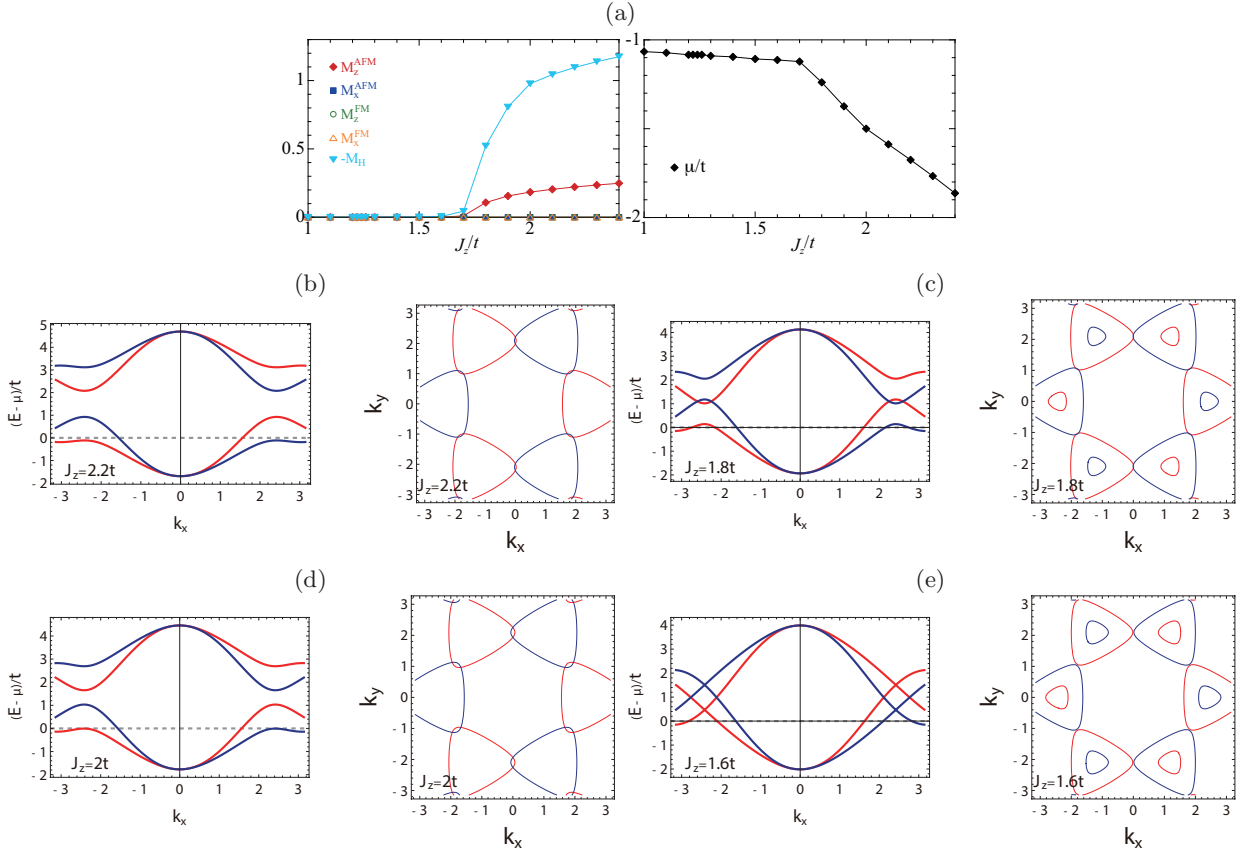


FIG. 5. (a) Order parameters and chemical potential as a function of J_z for $\lambda = 0.1t$ and $n = 0.79$. Band structures and corresponding Fermi surfaces along $k_y = 0$ for (b) $J_z = 2.2t$, (c) $J_z = 2t$, (d) $J_z = 1.8t$, (e) $J_z = 1.6t$. The red (blue) line corresponds to the spin up (down) component.

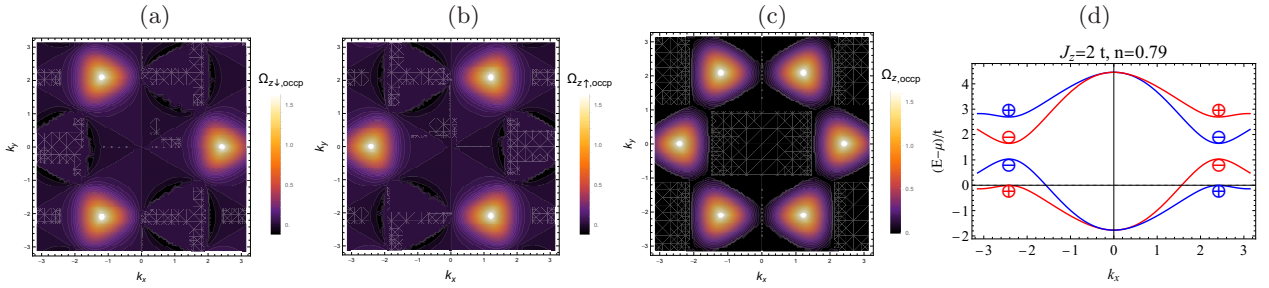


FIG. 6. Contour plots of the Berry curvatures (BC) of the occupied spin sub-bands with a spin projection (a) $\sigma = -1$ and (b) $\sigma = 1$. The total Berry curvature of the occupied bands is depicted in (c). The corresponding band structures are shown in (d) where the symbols \oplus and \ominus indicate the sign of the BC around the Dirac valleys. Calculations are done for $J_z = 2t$, $n = 0.79$. The BC is in unit of a^2 , where a is the distance between NN atoms.

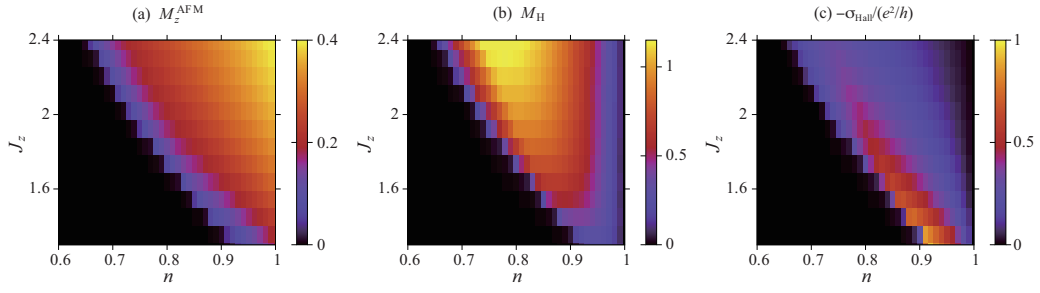


FIG. 7. Order parameters and anomalous Hall conductivity in the electron density n versus the interaction J_z for $\lambda = 0.1t$.

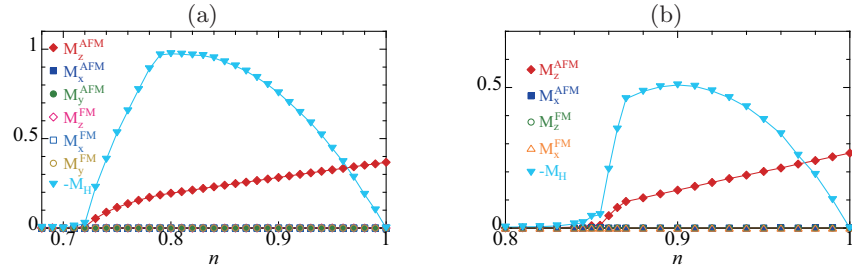


FIG. 8. Mean-field results with additional terms in Eq. (2) of the main text: (a) Rashba spin-orbit coupling [$\lambda_R = 0.1t$ at $J_z = 2t$] and (b) Hubbard U term [$U = 2.4t$ at $J_z = 0.4t$]. Here, $\lambda = 0.1t$.